IEEE Photonics Journal
An IEEE Photonics Society Publication

Open Access

Proposal and Fabrication of an Electrooptically Controlled Multimode Microresonator for Continuous Fast-to-Slow Light Tuning

Volume 6, Number 4, August 2014

Qingzhong Huang, Member, IEEE
Ge Song
Juguang Chen
Zhan Shu
Jinzhong Yu

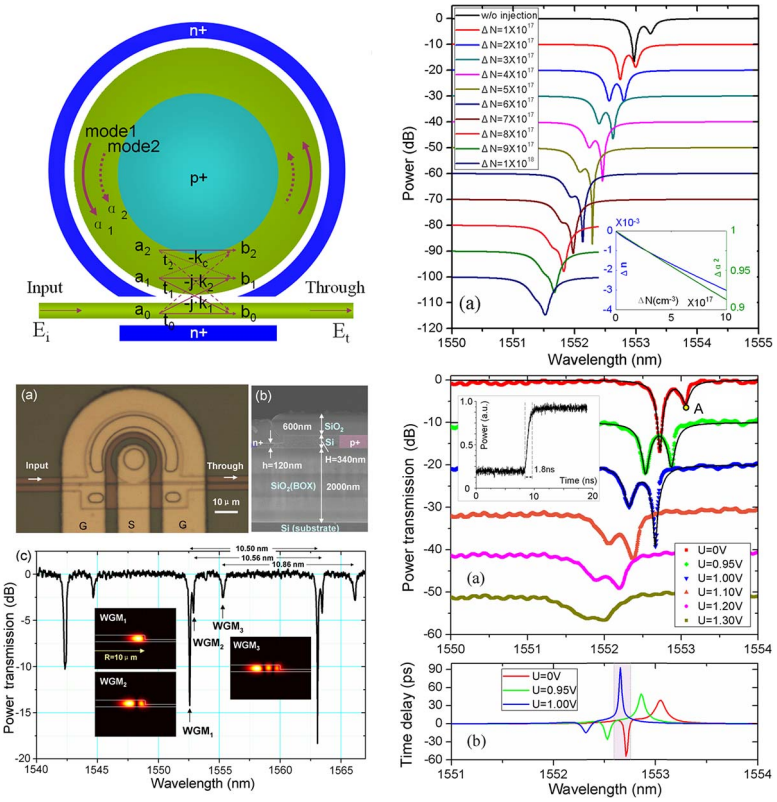

DOI: 10.1109/JPHOT.2014.2332473
1943-0655 © 2014 IEEE

Proposal and Fabrication of an Electrooptically Controlled Multimode Microresonator for Continuous Fast-to-Slow Light Tuning

Qingzhong Huang,[1] *Member IEEE*, Ge Song,[1] Juguang Chen,[1] Zhan Shu,[1] and Jinzhong Yu[1,2]

[1]Wuhan National Laboratory for Optoelectronics, Huazhong University of Science and Technology, Wuhan 430074, China
[2]Institute of Semiconductors, Chinese Academy of Sciences, Beijing 100083, China

DOI: 10.1109/JPHOT.2014.2332473

Manuscript received May 14, 2014; revised June 18, 2014; accepted June 18, 2014. Date of publication June 24, 2014; date of current version July 4, 2014. This work was supported in part by the National Natural Science Foundation of China under Grants 61006045, 61376055, and 61261130586, by the Major State Research Program of China under Grant 2013CB933303, and by the Major State Basic Research Development Program of China under Grant 2010CB923204.
Corresponding author: Qingzhong Huang (e-mail: huangqz@mail.hust.edu.cn).

Abstract: We propose a scheme to utilize a multimode microdisk resonator in silicon controlled through free-carrier injection for continuous fast-to-slow light tuning. Two nearby resonant modes are employed, i.e., undercoupling and overcoupling. The optical properties of a device are analytically investigated considering the resonance spacing, bandwidth, and density change of free carriers. Pulse propagation simulations are implemented, and the pulse delay/advance is studied for wavelengths between the two resonances. As the density of injected free carriers increases, a continuous transition from fast to slow light occurs for a range of wavelengths. Consequently, a microdisk resonator in silicon is experimentally realized with the desired two resonances, exhibiting electrooptical tuning with a fast response. The experimental results agree well with the simulation in power transmission, and the tunable time delay and advance are also predicted.

Index Terms: Microdisk resonator, slow light, silicon photonics, waveguide devices.

1. Introduction

For a long time, controlling the propagation speed of light has received considerable attention for its potential applications in optical data storage, optical communications, quantum computing, and information processing. Numerous studies have been done on tunable slow and fast light in dispersive materials using electromagnetically induced transparency and absorption [1], [2], coherent population oscillation [3]–[5], and stimulated Brillouin scattering [6], [7]. Continuously tunable fast-to-slow/slow-to-fast light recently has been carried out in highly doped erbium fibers [4], quantum-well semiconductor optical amplifiers [5], and chalcogenide glass waveguides [7]. The other method for obtaining slow and fast light is to utilize dispersive structures, such as Bragg gratings [8], [9], photonic crystal waveguides and cavities [10]–[13], microsphere resonators [14], [15], and microring resonators [16]–[26]. Silicon-on-insulator (SOI) is a promising platform for integrated nanophotonics due to the CMOS-compatible processing and high

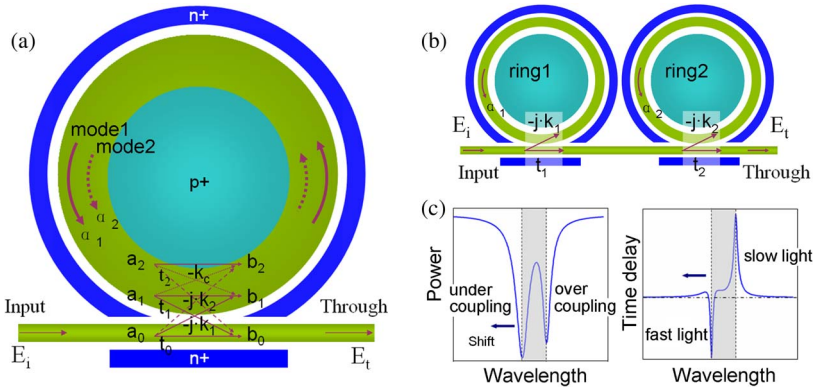

Fig. 1. (a) Schematic of a silicon based MDR integrated with an p-i-n junction. (b) Schematic of two cascaded microring resonators integrated with p-i-n junctions. (c) The operating principle diagram of continuous fast-to-slow light tuning using this structure.

index contrast. Fast and slow light in silicon have been studied and realized in dispersive structures, including Bragg gratings [8], photonic crystal slabs [10]–[13], and microring resonators [16]–[23]. The buffering can be tuned via thermo-optical method [12], [13], [16], [17] and electro-optical method [10], [18]–[22], while electro-optical tuning provides low power consumption and fast dynamic response.

Tunable fast-to-slow/slow-to-fast light has been achieved in a single-mode microresonator by varying the spacing gap [14], input polarization [24], and phase shift in a feedback waveguide [22]. However, with respect to continuous tuning, we have to manipulate two nearby resonant modes, supplied by a multimode resonator or coupled two resonators [21], [23], [25], [26]. It is noteworthy that the employment of multiple modes in a resonator is able to reduce the number of resonators required. In fact, two nearby modes are found in a single microring in the form of standing-wave modes caused by roughness-induced backscattering or coupler-induced localized backscattering [23], [25], [26]. Microdisk resonator (MDR) is known as a multimode structure [27]–[29], and here its multimode feature is utilized for continuously tunable fast-to-slow light. It is significant that the multiple traveling-wave modes in a MDR offer us another dimension other than bi-directional transmission to expand the ability of controlling light speed using a compact integrated device.

In this paper, we present a scheme to employ an electro-optically controllable multimode MDR in silicon for continuous fast-to-slow light tuning. The transition from fast to slow light is achieved by shifting two nearby travelling-wave modes. The optical properties of this structure are investigated using an analytical model, considering the resonance spacing, bandwidth, and density change of free-carriers. The propagation simulations indicate that the input pulses can be delayed or advanced for carrier wavelengths between the two resonances. As free carriers are injected into the resonator, a continuous transition from fast to slow light emerges for specific wavelengths. Consequently, we have realized a silicon MDR integrated with a p-i-n junction, and obtained the expected two resonances, which can be dynamically tuned in few nanoseconds. The experimental results agree with our modeling, and the time delay and advance are also simulated.

2. Device Structure and Theory

Fig. 1(a) shows the schematic structure of a silicon based MDR, which is laterally coupled with a bus waveguide to excite two whispering-gallery modes (WGMs) in the MDR simultaneously. The inner and outer sides of the MDR are heavily doped with boron and phosphorus, respectively, to form a p-i-n junction for injecting free electrons/holes into the optical guiding area.

As reported in [29], in the coupling region, the waveguide mode and WGM_1 (the first WGM)/WGM_2 (the second WGM) are evanescently and directly coupled, whereas WGM_1 and

WGM_2 are indirectly coupled through the waveguide. The transfer function of this structure is given by

$$T=\frac{b_0}{a_0}=\frac{t_0-e^{j\varphi_1'}\alpha_1'(k_1^2+t_0t_1)-e^{j\varphi_2'}\alpha_2'(k_2^2+t_0t_2)+e^{j(\varphi_1'+\varphi_2')}\alpha_1'\alpha_2'(2k_1k_2k_c+k_1^2t_2+k_2^2t_1-k_c^2t_0+t_0t_1t_2)}{1-e^{j\varphi_1'}\alpha_1't_1-e^{j\varphi_2'}\alpha_2't_2+e^{j(\varphi_1'+\varphi_2')}\alpha_1'\alpha_2'(-k_c^2+t_1t_2)} \tag{1}$$

where a_0 and b_0 are the input and output optical fields, respectively; $-jk_{1,2}$ is the field coupling coefficient between the waveguide mode and $WGM_{1,2}$; $-k_c$ is the field coupling coefficient between the two WGMs; $t_{0,1,2}$ is the field transmission coefficient. Here, $\varphi_{1,2}'=[4\pi^2R(n_{eff1,2}+\Delta n)]/\lambda$ is the round-trip phase shift, and $\alpha_{1,2}'=\alpha_{1,2}\Delta\alpha$ is the round-trip field attenuation for $WGM_{1,2}$, where Δn and $\Delta\alpha$ are the changes in effective mode index and round-trip field attenuation introduced by the free-carrier density change, respectively; R, $n_{eff1,2}$ and λ denote the MDR radius, effective mode index of $WGM_{1,2}$, and vacuum wavelength, respectively. When the p-i-n junction is forward biased, the densities of free holes and free electrons are changed equally and almost uniformly across the optical guiding area in MDR. Hence, the changes in effective mode index Δn and round-trip field attenuation $\Delta\alpha$ at 1550-nm wavelength are expressed as [30]

$$\Delta n=-\left[8.8\times10^{-22}\cdot\Delta N+8.5\times10^{-18}\cdot(\Delta N)^{0.8}\right] \tag{2}$$

$$\Delta\alpha=\exp(-1.45\times10^{-17}\cdot\Delta N\cdot L/2) \tag{3}$$

where ΔN is the density change of free electrons/holes (in units of cm^{-3}), and $L=2\pi R$ is the perimeter of MDR (in centimeters).

Then, we obtain the frequency-dependent time delay by

$$\tau_d=-\frac{d\Phi}{d\omega}=\frac{\lambda^2}{2\pi c}\cdot\frac{d\Phi}{d\lambda} \tag{4}$$

where $\phi=\arg(T)$ is the relative optical phase of transmission, ω is the light angular frequency, and c is the light speed in free space. Actually, the input data pulses contain large amounts of frequency components which are centered at the carrier frequency. Hence, the time delay (Δt) of data pulses passing through the device is close to τ_d, but not just the same as τ_d.

We calculate the output data pulses by doing the inverse Fourier transform of the output signal spectrum, which equals to the multiplying of device transmission and input signal spectrum [31].Thus, the intensity of the output data pulses in the time domain is described by

$$O(t)=|o(t)|^2=\left|FT^{-1}\{T(\omega)\cdot FT[i(t)]\}\right|^2 \tag{5}$$

where $i(t)$ and $o(t)$ are the amplitudes of the input and output data pulses in the time domain, respectively, and $T(\omega)$ is the device transmission as a function of angular frequency. Therefore, we can acquire the pulse delay (Δt) by comparing the output and input signals in the time domain.

As seen in Fig. 1(c), two resonances are excited at the same time in a MDR. One is under-coupling $(k_1^2+\alpha_1^2<1)$ for time advance, and the other is over-coupling $(k_2^2+\alpha_2^2>1)$ for time delay. While injecting the free carriers, the time delay spectrum blueshifts, and the device exhibits continuous fast-to-slow light tuning for certain wavelengths. Note that the resonance position and coupling efficiency between the waveguide mode and WGMs is adjustable through varying the structure dimensions (such as MDR radius, waveguide width, and spacing gap between the MDR and waveguide) [29], which is very important for obtaining the desired two resonances in a MDR. Ideally, power transmission remains constant while the time delay or

advance varies. However, resonator based delay lines are most effective on resonance, where the loss is largest [16]–[26]. Over-coupling or under-coupling can reduce the loss, but there is a delay-bandwidth-product for a single MDR. A solution to this tradeoff is to cascade multiple stages of MDRs [32].

Such two resonances are also achievable in two cascaded microring resonators (TCMRs), as depicted in Fig. 1(b), while one resonator is in the over-coupling regime, and the other resonator is in the under-coupling regime. The spacing between two microrings is large enough that they are not coupled to each other. Thus, the transfer function of this structure is given by

$$S = \frac{t_1 - \alpha_1' e^{j\varphi_1'}}{1 - \alpha_1' t_1^* e^{j\varphi_1'}} \cdot \frac{t_2 - \alpha_2' e^{j\varphi_2'}}{1 - \alpha_2' t_2^* e^{j\varphi_2'}} \tag{6}$$

where the symbols on the right hand side have almost the same meanings as those in (1), except that the subscripts 1 and 2 represent the first and second microrings instead of the WGMs in the single resonator structure of Fig. 1(a). Some comparison between the proposed device and TCMRs will be given in the following section.

3. Simulation and Analysis

We assume that the two resonant modes of a MDR and TCMRs both have $n_{eff1}L_1 = 183.249\ \mu$m, $n_{eff2}L_2 = 172.411\ \mu$m, $k_1^2 = 0.045$, $k_2^2 = 0.060$, $\alpha_1^2 = 0.940$, and $\alpha_2^2 = 0.980$. This results in the first resonance to be under-coupled, and the second resonance to be over-coupled. In this case, minor difference is found between the two structures in power, phase, and time delay, as shown in Fig. 2. However, as the optical distance of WGM_2 $(n_{eff2}L_2)$ decreases, the right (second) resonance moves towards the left (first) resonance, and the output spectra for two structures becomes increasingly different. Here we are concerned about the variation of extinction ratio (ER) and time delay/advance for the left resonance. For the MDR, the resonance ER decreases, and it switches from superluminal to subluminal propagation, when the resonance spacing is reduced, as seen in Fig. 2(a) and (e). In contrast, for the TCMRs, the resonance ER increases, and the time advance keeps decreasing, when the two resonances get close to each other, as seen in Fig. 2(b) and (f). We attribute it to the fact that the mode coupling and competition between the two WGMs in a MDR are non-negligible as they are both on resonance, whereas the two resonant modes in TCMRs are independent and the overall output is just the superposition of two individual resonances. That is to say, when the two resonances are separated, the MDR and TCMRs have almost the same output power, phase, and time delay. However, the MDR configuration is more compact in size and has lower power consumption, because of the sharing of injected free carriers for the two WGMs of the single resonator structure of Fig. 1(a). In addition, it is interesting that fast-to-slow light tuning is also achievable in such a MDR by only adjusting the position of the right resonance.

In the presence of $k_1^2 + \alpha_1^2 < 1$, we tune the bandwidth while roughly maintaining the maximum value of time advance for one resonance by altering k_1^2 and α_1^2, though the associated power bandwidth and ER may change obviously, as seen in Fig. 3. When the bandwidth of time advance is very small, an oscillation appears in the time delay spectrum between the two resonant peaks, as shown in Fig. 3(b). As k_1^2 increases and α_1^2 decreases, this bandwidth is enlarged, and then the oscillation becomes small and even disappears. We know that, for an under-coupled resonance, abnormal dispersion occurs at the resonance, intervened between two normal dispersion regions, which results in two small time-delay ripples on each side of the time-advance peak. However, if the ratio of time-advance bandwidth to resonance spacing is relatively large, the time-delay ripple between the two resonant wavelengths will gradually fade away. It is provable that the variation in time delay spectrum is similar as enlarging the bandwidth(s) of the other resonance or both two resonances. In this case, the time delay varies with the wavelength monotonously between the two resonances, implying a monotonous and continuous fast-to-slow light tuning as the spectrum shifts.

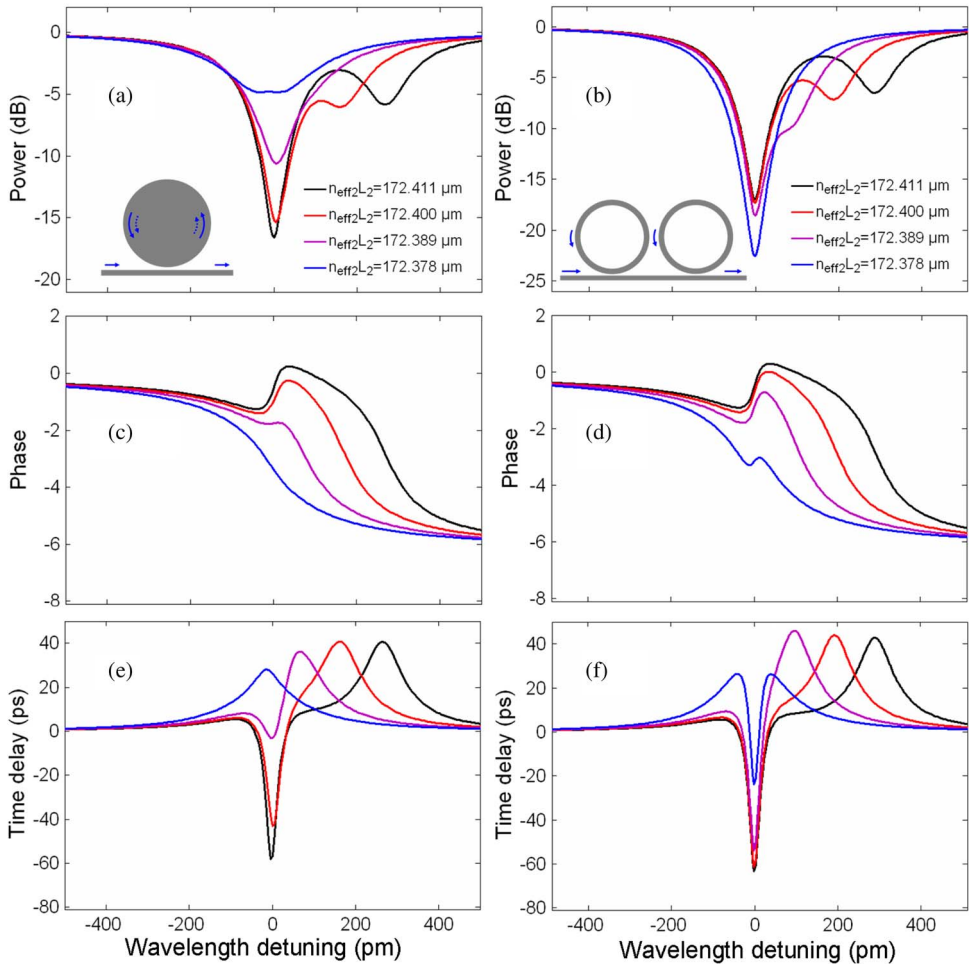

Fig. 2. The power (a), phase (c), and time delay (e) spectra of a MDR and the power (b), phase (d), and time delay (f) spectra of TCMRs with a varied resonance spacing.

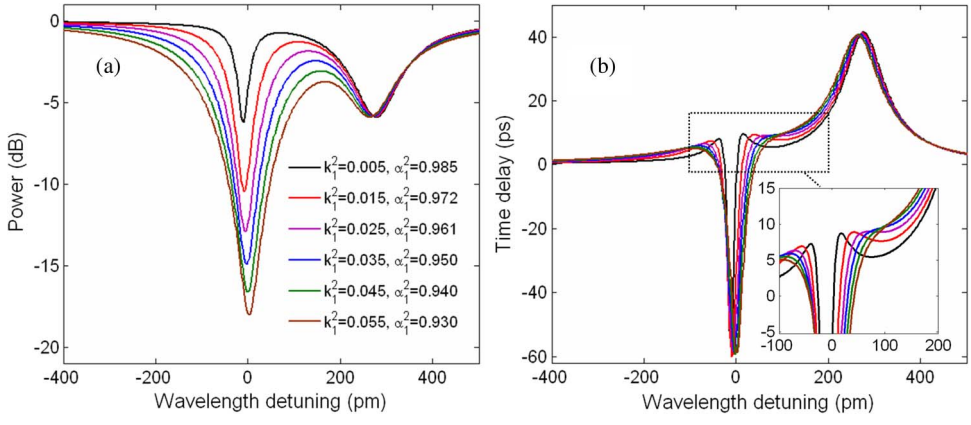

Fig. 3. The power (a) and time delay (b) spectra of a MDR with a varied resonant bandwidth.

To study the impact of free-carrier injection, the power, phase and time delay spectra for various ΔN (from 0 to 1×10^{18} cm^{-3}) are simulated and given in Fig. 4(a)–(c). The density change of free carriers depends on the bias voltage on the p-i-n junction, as described in [33]. In the

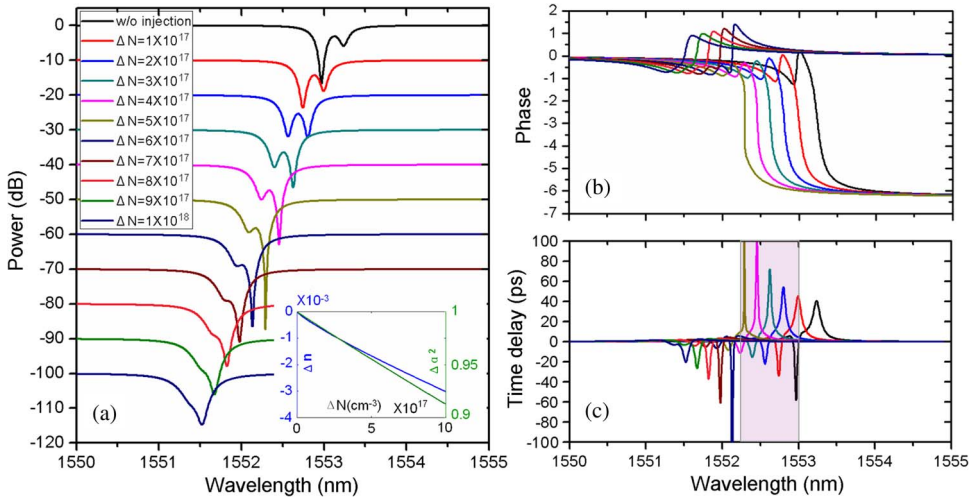

Fig. 4. The power (a), phase (b), and time delay (c) spectra for various ΔN. Inset in (a): the effective mode index and round-trip power attenuation as a function of ΔN.

beginning, the resonances of WGM_1 and WGM_2 are in the under-coupling and over-coupling regimes, respectively, without free-carrier injection. As ΔN increases, the two resonances both blueshift, while the WGM_2 resonance first approaches critical-coupling and then becomes under-coupling. That is because the effective mode index and round-trip power attenuation both decrease with the density change of free carriers [see the inset of Fig. 4(a)], and $(k_2^2 + \alpha_2^2)$ is lowered to less than 1. It is expectable that the continuous tuning from fast to slow light can be realized in the wavelength range covered by the shifting of two resonances, due to an increase of ΔN, as seen in Fig. 4(c).

To examine the pulse delay and output signal waveform, we choose a MDR with power and time delay spectra given in Fig. 5(a). The MDR is passed through by non-return-to-zero (NRZ) and return-to-zero (RZ, duty cycle: 0.30) signals with 2nd order super-Gaussian and Gaussian envelops, respectively, and the carrier wavelengths are set typically to the five positions labeled in Fig. 5(a). The pulse delay/advance is measured by comparing the output and input pulses shown in Fig. 5(c), where the waveforms are normalized by the flat top of the "1" level. Table 1 shows the simulated results of pulse delay for 1 and 5-Gbps NRZ/RZ signals. In general, we observe that the pulse delay/advance of NRZ signal is larger than that of RZ signal, and the pulse delay/advance of high speed signal is smaller than that of low speed signal. The pulse delay is determined by the overlap of signal spectrum and time delay spectrum. Since the bandwidth of RZ signal is larger than that of NRZ signal at the same rates, more frequency components of RZ signal exceed the range of large time delay/advance, resulting in smaller time delay/advance, as seen in Fig. 5(b). The influence of data rates on time delay/advance also can be analyzed in the same way. Fig. 5(c) shows that the pulse envelope is well preserved both in intensity and shape for low speed signals, whereas more distortion is observed in the output waveform for high speed NRZ signals at a resonant carrier wavelength. For a delayed pulse, we see a small oscillation in the leading edge and a sharp overshoot in the trailing edge, and the output pulse width becomes a little wider. Nevertheless, for an advanced pulse, the situation is opposite: the sharp overshoot and small oscillation appear in the trailing and leading edges, respectively, and the pulse width becomes a little narrower. The waveform distortion is mainly attributed to the third-order dispersion (TOD) of this device, which is the largest at the resonant wavelength, as shown in the inset of Fig. 5(a).

For a wavelength on the left side of two resonances, it experiences under-coupling (fast light) and over-coupling (slow light) in succession, when the two resonant peaks move leftward and pass through it. In Fig. 6, the tuning of time delay is shown as a function of free-carrier density change for specific wavelengths. Here, the solid lines are for a MDR with $k_1^2 = 0.045$,

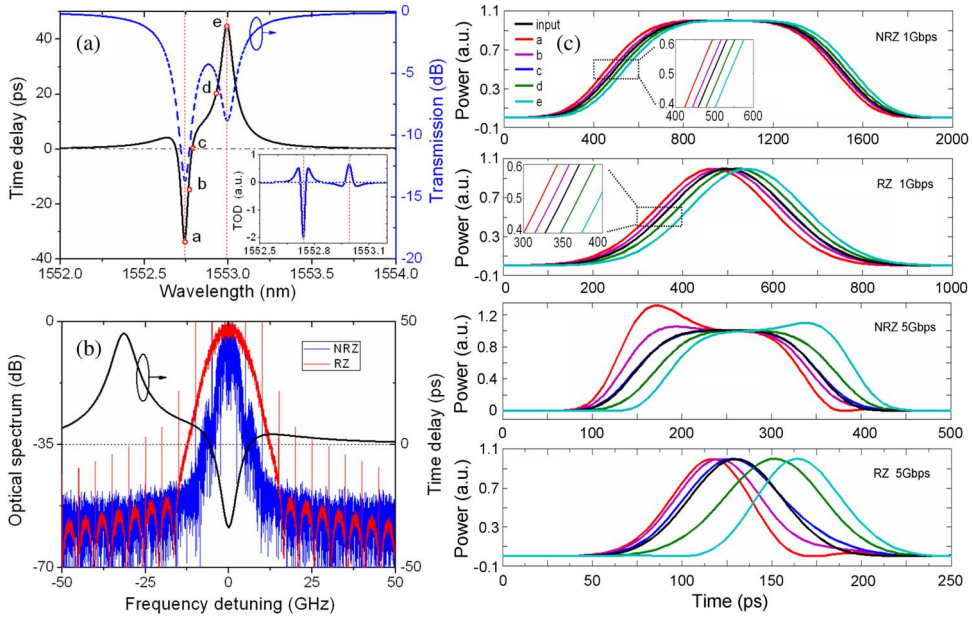

Fig. 5. (a) The power and time delay spectra of a selected MDR. Inset: the MDR's TOD as a function of wavelength. (b) The optic al spectra of RZ and NRZ input signals at 5 Gbps; the black line represents the time delay spectrum. (c) The output signals in the time domain for input signals (black lines) at 1 and 5 Gbps with the carrier wavelengths corresponding to the five points.

TABLE 1

The time delay and pulse delay for the five typical wavelengths, in picoseconds

	T_d	Δt (NRZ 1G)	Δt (RZ 1G)	Δt (NRZ 5G)	Δt (RZ 5G)
a	-33.2	-33.0	-27.6	-23.4	-14.4
b	-14.7	-13.5	-13.1	-12.5	-9.6
c	0	0.6	0	-0.8	-2.0
d	20.3	20.0	19.8	20.3	21.1
e	44.8	44.7	44.5	41.1	35.4

$k_2^2 = 0.060$, $\alpha_1^2 = 0.940$, and $\alpha_2^2 = 0.980$, while the dashed lines are for a relatively large-bandwidth MDR with $k_1^2 = 0.060$, $k_2^2 = 0.090$, $\alpha_1^2 = 0.920$, and $\alpha_2^2 = 0.950$. It is observed that the time delay can be tuned continuously from negative (i.e. time advance) to positive values for a range of wavelengths by raising the density change. Conversely, slow-to-fast light tuning is also obtainable by reducing the density change. With the aim of achieving continuous and monotonous fast-to-slow light tuning, we should choose a proper variation range for free-carrier density change, which is dependent on wavelength. Furthermore, by comparing the solid and dashed lines, we find that the maximum value of time delay/advance is smaller, and the transition between two extremes requires a minor variation of density change, for a MDR with larger resonance bandwidths.

4. Fabrication and Test

The proposed structure was fabricated on a SOI wafer having a 340-nm-thick top silicon layer and a 2-μm-thick buried oxide layer. The fine pattern was first defined by electron beam lithography, and then transferred to silicon with a depth of 220 nm by inductively coupled plasma etching. The MDR radius is 10 μm, the spacing between the MDR and the waveguide is

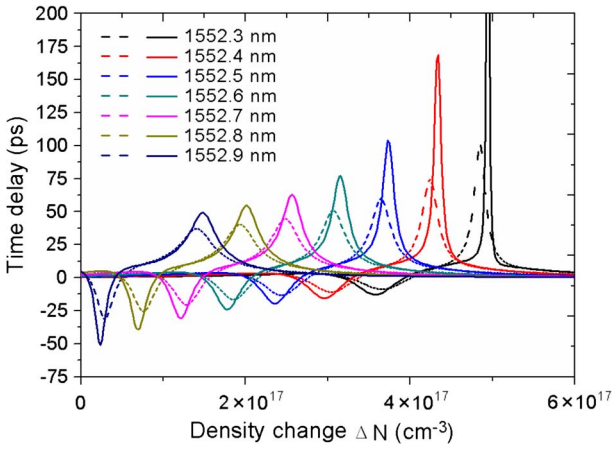

Fig. 6. The tuning from fast light to slow light using a MDR by changing the free-carrier density for specific wavelengths, keeping $n_{eff1}L_1 = 183.249\ \mu$m, and $n_{eff2}L_2 = 172.411\ \mu$m.

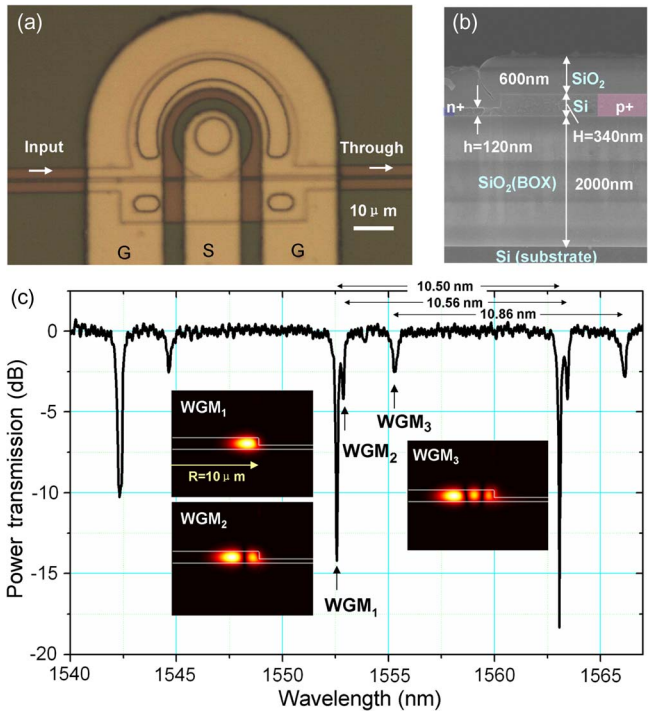

Fig. 7. (a) Microscope image of the fabricated silicon MDR integrated with a p-i-n junction. (b) Cross-sectional view SEM image of the MDR rim. (c) The normalized power transmission of the device without bias. Inset: Simulated E-field profiles of WGM_1, WGM_2, and WGM_3 in the MDR.

210 nm, and the waveguide width is 350 nm. The highly-doped n+ and p+ regions (both 1×10^{20} cm^{-3}) are formed 1 μm and 2.5 μm away from the MDR rim, respectively. A 600 nm-thick SiO_2 film was deposited on the MDR for electrical isolation, and NiSi silicide was used for ohmic contact. The aluminum contact pads of 1 μm in thickness were defined using photolithography and evaporation followed by lift-off. The fabricated structure is shown in Fig. 7(a) and (b). After that, the power transmission was measured for quasi-TE polarization. Three low-order WGMs have been effectively triggered in the MDR as seen in Fig. 7(c). The nearby two resonances are identified as WGM_1 and WGM_2 based on the measured free spectrum ranges. As

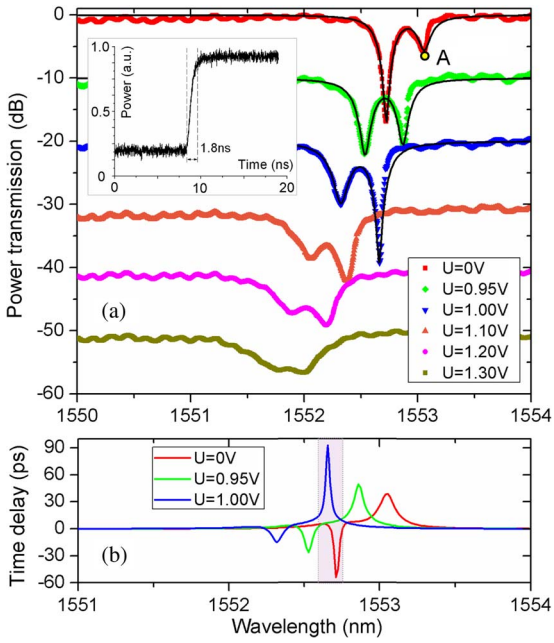

Fig. 8. (a) The measured transmissions (solid dots) and several theoretical fits (solid lines) under various biases. The best-fit parameters are set as $k_1^2 = 0.045$, $k_2^2 = 0.062$, and $(n_{eff1}, n_{eff2}, \alpha_1^2, \alpha_2^2) = (2.91604, 2.74368, 0.940, 0.980)$, $(2.91569, 2.74335, 0.925, 0.965)$, $(2.91529, 2.74298, 0.909, 0.948)$ for the biases of 0 V, 0.95 V, and 1.00 V, respectively. Inset: Transient response of the output power as the applied voltage switched from -1.0 V to 1.0 V. (b) The predicted time delay spectra for 0 V, 0.95 V, and 1.00 V.

predicted previously, the resonance ER of WGM_1 becomes lower when the two resonances get closer to each other, and the lowest when they coincide. It is found that the effective mode index of the waveguide mode TE_0 (n_{eff0} of $\sim$2.65) is between that of WGM_2 (n_{eff2} of $\sim$2.74) and WGM_3 (n_{eff3} of $\sim$2.60) at 1550-nm wavelength, which leads to stronger $TE_0 - WGM_2$ coupling and $TE_0 - WGM_3$ coupling than $TE_0 - WGM_1$ coupling.

Fig. 8(a) shows the measured power transmissions under various biases. The resonances of WGM_1 and WGM_2 exhibit quality (Q) factors of 6,700 and 8,600 and ERs of 16.8 dB and 5.6 dB upon 0 V bias, respectively. Increasing the bias, the two resonances blueshift, and the Q factors of WGMs and ER of WGM_1 both decrease monotonously, while the ER of WGM_2 increases at first and then starts to fall. This trend agrees with the simulation results in Fig. 4(a). It is found that the electro-optical tuning only consumes 0.62 mW of dc power when applying a bias of 1.00 V. By fine tuning the bias and observing the variation of ER, the resonances have been identified to be over-coupling or under-coupling. Several transmissions are fitted by the analytical model, and nice fits are observed in Fig. 8(a). The experimental results prove that both n_{eff} and α^2 decrease with the bias voltage, since more free carriers are generated under a higher forward bias. According to the measured results, the carrier density changes are estimated to be about 2×10^{17} cm^{-3} and 4×10^{17} cm^{-3} at 0.95 V and 1.0 V, respectively, which agree with the numerical simulation for our p-i-n structure. Moreover, the simulation reveals that the carrier density change varies almost linearly at 2.4×10^{17} cm^{-3}/0.1 V as the voltage changes between 0.9 V and 1.2 V. Then, we probed the output power at a fixed wavelength [point A in Fig. 8(a)] under electrical pulses, and the transition occurs in 1.8 ns as the voltage is switched from -1.0 V to 1.0 V (see the inset), implying an ability of ultra-fast fast-to-slow light tuning. Furthermore, we predict the time delay spectra for this device using the fitting parameters. The time delay spectrum shifts with the bias, and the maximum values of tunable time delay and advance are $\sim$90 and $\sim$50 ps, respectively, as shown in Fig. 8(b). The tuning range of time delay for a wavelength also can be predicted. For example, at 1552.71 nm, the time delay

is tuned from about −50 ps to 70 ps to the maximum as the voltage changes from 0 V to 1.0 V. Note that the wavelength range of tuning is practically limited by the increasing heat generated by the rising power consumption, since thermo-optic effect makes resonances redshift.

5. Conclusion

In summary, we present an approach to achieve continuously tunable fast-to-slow light on a chip by controlling a silicon multimode MDR with two nearby resonances electro-optically. For this structure, the optical properties including power, phase and time delay are investigated analytically, and the pulse propagation simulations are also performed and exhibit time delay or advance without significant distortion. It is observed that the transition from fast to slow light is continuous for a range of wavelengths when the MDR is injected with free carriers. Then, an electro-optically controllable MDR was fabricated with the desired two resonant modes, which can be tuned with sub-milliwatt power in few nanoseconds. The modeling fits the experimental results well, and the potential time delay and advance are given. It is expected that the proposed device will find more applications for on-chip optical buffering and optical information technology in the future.

References

[1] L. V. Hau, S. E. Harris, Z. Dutton, and C. H. Behroozi, "Light speed reduction to 17 metres per second in an ultracold atomic gas," *Nature*, vol. 397, no. 6720, pp. 594–598, Feb. 1999.
[2] Y. S. Lee, H. J. Lee, and H. S. Moon, "Phase measurement of fast light pulse in electromagnetically induced absorption," *Opt. Exp.*, vol. 21, no. 19, pp. 22 464–22 470, Sep. 2013.
[3] P.-C. Ku *et al.*, "Slow light in semiconductor quantum wells," *Opt. Lett.*, vol. 29, no. 19, pp. 2291–2293, Oct. 2004.
[4] O. G. Calderón *et al.*, "Propagation-induced transition from slow to fast light in highly doped erbium fibers," *Phys. Rev. A*, vol. 78, no. 5, pp. 053812-1–053812-8, Nov. 2008.
[5] P. K. Kondratko and S.-L. Chuang, "Slow-to-fast light using absorption to gain switching in quantum-well semiconductor optical amplifier," *Opt. Exp.*, vol. 15, no. 16, pp. 9963–9969, Aug. 2007.
[6] L. Thevenaz, "Slow and fast light in optical fibres," *Nature Photon.*, vol. 2, no. 8, pp. 474–481, Aug. 2008.
[7] R. Pant *et al.*, "Photonic-chip-based tunable slow and fast light via stimulated Brillouin scattering," *Opt. Lett.*, vol. 37, no. 5, pp. 969–971, Mar. 2012.
[8] S. Khan, M. A. Baghban, and S. Fathpour, "Electronically tunable silicon photonic delay lines," *Opt. Exp.*, vol. 19, no. 12, pp. 11 780–11 785, Jun. 2011.
[9] H. Shahoei and J. Yao, "Continuously tunable slow and fast light by using an optically pumped tilted fiber Bragg grating written in an Erbium/Ytterbium co-doped fiber," *Photon. Technol. Lett.*, vol. 24, no. 10, pp. 818–820, May 2012.
[10] Y. A. Vlasov, M. O'Boyle, H. F. Hamann, and S. J. McNab, "Active control of slow light on a chip with photonic crystal waveguides," *Nature*, vol. 438, no. 7064, pp. 65–69, Nov. 2005.
[11] T. Baba, "Slow light in photonic crystals," *Nature Photon.*, vol. 2, no. 8, pp. 465–473, Aug. 2008.
[12] T. Gu *et al.*, "Deterministic integrated tuning of multicavity resonances and phase for slow-light in coupled photonic crystal cavities," *Appl. Phys. Lett.*, vol. 98, no. 12, pp. 121103-1–121103-3, May 2011.
[13] N. Ishikura *et al.*, "Photonic crystal tunable slow light device integrated with multi-heaters," *Appl. Phys. Lett.*, vol. 100, no. 22, pp. 221110-1–221110-3, May 2012.
[14] K. Totsuka and M. Tomita, "Slow and fast light in a microsphere-optical fiber system," *J. Opt. Soc. Amer. B*, vol. 23, no. 10, pp. 2194–2199, Oct. 2006.
[15] K. Totsuka and M. Tomita, "Dynamics of fast and slow light propagation through a microsphere-optical-fiber-system," *Phys. Rev. E*, vol. 75, no. 1, pp. 016610-1–016610-5, Jan. 2007.
[16] F. Morichetti *et al.*, "A reconfigurable architecture for continuously variable optical slow-wave delay lines," *Opt. Exp.*, vol. 15, no. 25, pp. 17 273–17 282, Dec. 2007.
[17] F. Shinobu, N. Ishikura, Y. Arita, T. Tamanuki, and T. Baba, "Continuously tunable slow-light device consisting of heater-controlled silicon microring array," *Opt. Exp.*, vol. 19, no. 14, pp. 13 557–13 564, Jul. 2011.
[18] S. Manipatruni, P. Dong, Q. Xu, and M. Lipson, "Tunable superluminal propagation on a silicon microchip," *Opt. Lett.*, vol. 33, no. 24, pp. 2928–2930, Dec. 2008.
[19] X. Luo, H. Chen, and A. W. Poon, "Electro-optical tunable time delay and advance in silicon microring resonators," *Opt. Lett.*, vol. 35, no.17, pp. 2940–2942, Sep. 2010.
[20] J. Cardenas *et al.*, "Wide-bandwidth continuously tunable optical delay line using silicon microring resonators," *Opt. Exp.*, vol. 18, no. 25, pp. 26 525–26 534, Dec. 2010.
[21] S. Manipatruni, C. B. Poitras, and M. Lipson, "Electro-optically tunable delay on a silicon micro-chip," presented at the Conf. Lasers Electro-Opt./Int. Quantum Electron., OSA Tech. Dig. (CD), Baltimore, MA, USA, 2009, paper CThBB4.
[22] S. Feng, X. Luo, S. Du, and A. W. Poon, "Electro-optical tunable time delay and advance in a silicon feedback-microring resonator," *Opt. Lett.*, vol. 36, no. 7, pp. 1278–1280, Apr. 2011.
[23] T. Wang *et al.*, "Pulse delay and advancement in SOI microring resonators with mutual mode coupling," *J. Lightw. Technol.*, vol. 27, no. 21, pp. 4734–4743, Nov. 2009.

[24] C. Fietz and G. Shvets, "Simultaneous fast and slow light in microring resonators," *Opt. Lett.*, vol. 32, no. 24, pp. 3480–3482, Dec. 2007.
[25] T. Y. L. Ang and N. Q. Ngo, "Tunable fast and slow light in a traveling wave microresonator via interaction of intracavity backscattering with dual contrapropagating inputs," *J. Opt. Soc. Amer. B*, vol. 27, no. 12, pp. 2774–2783, Dec. 2010.
[26] T. Y. L. Ang and N. Q. Ngo, "Harnessing coupler-induced localized backscattering for enhanced fast and slow light performances in a traveling wave microresonator," *J. Opt. Soc. Amer. B*, vol. 27, no. 12, pp. 2639–2647, Dec. 2010.
[27] M. Borselli, T. J. Johnson, and O. Painter, "Measuring the role of surface chemistry in silicon microphotonics," *Appl. Phys. Lett.*, vol. 88, no. 13, pp. 131114-1–131114-3, Mar. 2006.
[28] Y.-S. Choi *et al.*, "Dispersive phase response in optical waveguide-resonator system," *Appl. Phys. Lett.*, vol. 90, no. 19, pp. 191108-1–191108-3, May 2007.
[29] Q. Huang, "Electromagnetically induced transparency-like effect in a two-bus waveguides coupled microdisk resonator," *Opt. Exp.*, vol. 22, no.3, pp. 3219–3227, Feb. 2014.
[30] Q. Huang, X. Zhang, J. Xia, and J. Yu, "Systematic investigation of silicon digital 1×2 electro-optic switch based on a microdisk resonator through carrier injection," *App. Phys. B*, vol. 105, no. 2, pp. 353–361, Nov. 2011.
[31] P. Acebal, L. Carretero, and S. Blaya, "Group-delay control in two-port devices with dual input," *IEEE Photon. J.*, vol. 5, no. 2, pp. 7900610-1–7900610-10, Apr. 2013.
[32] J. Yang *et al.*, "Continuously tunable, wavelength-selective buffering in optical packet switching networks," *IEEE Photon. Technol. Lett.*, vol. 20, no. 12, pp. 1030–1032, Jun. 2008.
[33] P. D. Hewitt and G. T. Reed, "Improving the response of optical phase modulators in SOI by computer simulation," *J. Lightw. Technol.*, vol. 18, no. 3, pp. 443–450, Mar. 2000.